

Hydrogel-Elastomer Composite Stretchable Sensors for the Detection of Asymmetric Deformations in a Soft Manipulator

David Hardman¹, Ryman Hashem¹ and Fumiya Iida¹

Abstract—We present an easy-to-fabricate soft composite strain sensor, made from the combination of a gelatin/glycerol hydrogel and silicone. We illustrate the sensor’s customizability and repeatability by iteratively designing a sensor morphology for deployment in an underactuated soft robotic manipulator, which requires the sensing of asymmetric deformations in a soft skin. The high sensitivity of the final morphology enables transient responses to be used to infer the actuator’s state in conjunction with the applied pressure values.

By fully encasing the sensorized hydrogel in silicone, we also demonstrate improvements in durability over the un-encased sensor, and experimentally find the sensors capable of withstanding over 200% strain before the onset of delamination. This method facilitates the sensor’s use in a wide range of soft robotic actuators: we present its ability to respond to repeated, incremental, and oscillating stimuli in a soft manipulator. The sensor can easily be implemented on soft actuators without the need for redesigning the actuators’ morphology.

I. INTRODUCTION

The fast-growing field of soft robotics has led to the emergence of biomimetic actuators which can be deployed into hostile environments, work safely alongside humans, and manipulate delicate objects, such as foodstuffs [2]. To integrate these developments into fully soft and compliant robotic systems, soft and flexible sensors must also be incorporated [3], using customizable sensor morphologies to return detailed information about the nonlinear continuum deformations of the actuators and their environments.

Typically, elastomer-based sensing techniques for soft robots are based on the incorporation of piezoelectric conductive fillers into silicones, which can be cast, or injection moulded as desired [4], [5], [6]. Where custom sensor morphologies are required, fibrous sensors or liquid channels can be embedded into a surrounding elastomer matrix [7], [8], [9], [10]. Alternatively, piezoelectric conductive filaments can be used in conjunction with fused deposition modelling [11], though such approaches often introduce delamination failure mechanisms due to interfacial stresses between the different stiffness materials.

The highly stretchable nature of hydrogels and their tunable compositions makes them an appealing choice for soft robotics [12], [13] and soft sensors [14], [15], [16], [17]. Gelatin-based actuators have been explored for their ease of fabrication, biocompatibility, and edibility [18], [19], [20], [21]. The inclusion of glycerol as a plasticizer that bonds with water molecules reduces the rate at which the gel dries out, and such compositions can be shown to remain stable and flexible for many months [22]. Further studies demonstrate the biodegradation of gelatin/glycerol hydrogels in warm water and soil [23], [24]. Their low melting point enables straightforward extrusion-based printing [25]; a technique approach which

facilitates the manufacture of custom strain sensors [26], [27], and which has been well-explored in conjunction for hydrogel sensors and actuators. [28], [29], [30], [31]. In addition, the self-healing properties of many hydrogels provide a route for damage recovery in deployable soft robotics [32], [33], and can be incorporated into the manufacture of soft sensors [34], [35].

In this work, we investigate a cheap and easy to use method of a single composite sensor that can provide additional information for soft robots and actuators. We examine the performance of composite soft sensors. It is fabricated from an ionically sensorized self-healing gelatin/glycerol hydrogel, which was previously introduced and characterized by the authors [22], and platinum-catalyzed silicones, a widely used silicone in soft robotic manufacture. By coupling the two low-stiffness materials, we demonstrate how our strain sensors can reliably and repeatably respond to strains of at least 200% before delamination occurs. Also, the sensor benefits from the extrudability of the hydrogel in the straightforward manufacture of custom morphologies. By encasing the hydrogel in silicone, the bond between the two materials is significantly improved rather than forming a simple two-layer composite. Moreover, the sensor’s baseline resistance differences caused by a continued equilibrium with environmental humidity are reduced.

We validate the design of our composite sensor (Fig. 1) and highlight its use in the design and development of custom morphologies by introducing a biomimetic soft actuator based on a peristaltic stomach contraction (Fig. 1) [1]. As demonstrated in the authors’ previous work, this multi-degree-of-freedom actuator can be used to facilitate in-hand manipulation of small objects, using the bistability of its fingers to rotate objects smoothly about an axis. Each of the five fingers is pneumatically actuated. Still, the underactuation of the system means that the five pressures are insufficient to determine the soft actuator’s state. Upon encountering an object, the fingers undergo bifurcation (Fig. 1). The direction in which the fingers bifurcate is undetectable from the magnitudes of the applied pressures. We previously investigated the placement of two thermoplastic sensors over the soft finger for detecting bifurcation. Although the sensor was able to identify the bifurcation, the sensor stretchability was half of the required for the actuator, and coupling the materials was not achievable.

We investigate the use of a single composite sensor in delivering sensing feedback of finger positions through an encased hydrogel channel inside the actuator’s skin (Fig. 1). The out-of-plane deformations which must be sensed to obtain proprioceptive data necessitate highly stretchable sensors which do not impede the motion or function of the actuator.

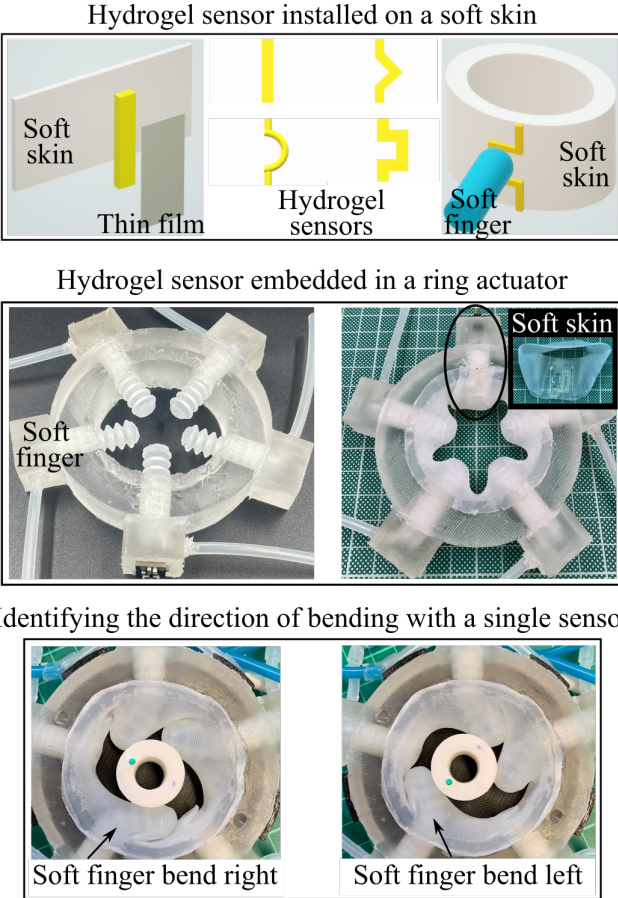


Fig. 1: The concept of embedding hydrogel sensor in a soft actuator. Different shapes of sensors are examined to identify the maximum strain. A thin film is placed over the sensor to ensure attachment to the soft skin. The soft skin with a hydrogel sensor is placed on the soft ring actuator from [1]. The sensor is placed directly in front of the soft finger. The proposed different shapes of sensors are to identify the bending direction of the soft fingers, left or right. Also, the sensors can detect the displacement of the soft finger.

In addition, directionality data is desired to infer the direction of rotation of the manipulated object; we use the customisability of our composite sensors to explore the advantages and disadvantages of four different sensor morphologies as a preliminary demonstration of this asymmetric sensing.

We chose this actuator to validate our method of implementing a simple hydrogel sensor as the actuator has two degrees of freedom (elongation and bending) and serves different applications such as in-hand manipulation in [36] and a soft stomach robot [1]. The hydrogel sensor is preferred for its cheap, simple to make and easy to shape on soft robots.

Firstly (Sections II-A & II-B), we determine the composite sensor volume fractions most suitable for our application, testing the responses of several sensorized channel geometries to small (30%) and large ($\geq 200\%$) applied strains, and a channel 4 mm wide and 3 mm high is selected for additional experimentation. The benefits of silicone encasing to prevent delamination and facilitate healing are also explored; though

the composite sensor's silicone casing is not capable of recovering from damages, we demonstrate its use in maintaining the sensor morphology during thermal healing of the sensorized hydrogel.

After choosing a suitable volume fraction, we compare four sensor morphologies for the detection of asymmetric deformations in the soft actuator (Section II-C). The 4×3 mm geometry is used to fabricate transverse and longitudinal sensors which incorporate the four morphologies. Based on the sensor responses and failure mechanisms, the ‘square’ morphology is found to be the best choice.

Finally, this morphology is incorporated into the actuator (Section II-D), where it is shown to clearly and repeatedly respond as designed to out of plane deformations and asymmetries. We demonstrate how analyzing the transient responses of the sensor provides additional information about the state of the actuator and any objects it is manipulating.

II. RESULTS AND DISCUSSION

A. Composite Material

Fig. 2a shows the standard dimensions of a geometric test sample, used to determine the values of $w \times t$ to be used as the basis of more complex morphologies. A sensorized gelatin/glycerol hydrogel channel of the specified dimensions is cast onto the 1 mm thick soft skin and is enclosed using a thin silicon layer. The benefits of the fully enclosed channel are evident in the accompanying video. The unenclosed channel quickly delaminates from the soft skin, whilst the enclosed channel continually undergoes applied strain cycles. Once cured, Fig. 2b shows the response of the 4×2 mm geometry to applied strain trapezoids of 300%. The stretchable composite easily withstands and responds clearly and repeatably to the significant deformations, drifting by only 0.009 V over the 4 repetitions (less than 3% of the average response magnitude). At this rate of strain (See Section IV), no overshoot is noticeable in the sensor responses, though small levels of material relaxation are apparent between the trapezoids. Though the strain trapezoids are applied linearly, the sensor responses contain clearly nonlinear regions at higher strains, even when the signals are converted to resistive values. This contrasts with the highly linear responses of the unconstrained hydrogel in previous studies [22], suggesting that the interfacial forces acting between the hydrogel and its soft skin casing cause the composite material to behave uniquely at higher strains. In addition, the silicone holds the hydrogel in place if the damage is inflicted, such that an applied heat source can be used to heal the internal hydrogel without a loss of morphology, as demonstrated in Fig. 2c and the accompanying video. In this example, both the hydrogel and silicone are cut with a scalpel so that the sensor stops responding. A rework station’s air gun is then used to heat the sensor in the area of damage locally. The composite remains weakened, since the silicone does not heal, but this heat source is sufficient to recover the strain sensitivity over the 50% strain trapezoids applied: a property that could be used to temporarily deal with a damaged soft robot until the sensor is fully repaired.

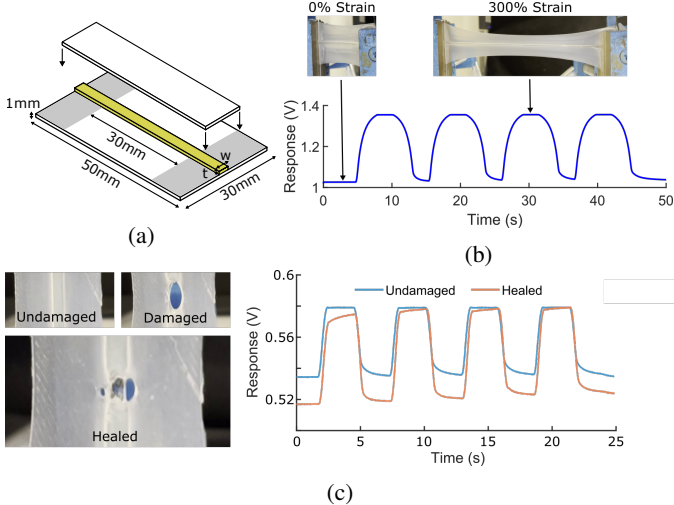


Fig. 2: a) Arrangement of the geometric samples. A $w \times t$ mm sensorized hydrogel strip (yellow) is sandwiched between soft skin and a thin silicon layer, creating a 50×30 mm test sample. The clamped area is indicated by the shaded region. b) Response of the 4×2 mm sensorized sample to applied strains of 300%. Note the non-zero y-intercept. c) Healing of the sensorized hydrogel through applied heat. Though the encasing soft skin does not heal, it holds the broken hydrogel channels together during heating to ensure the recovery of the sensor response to the 50% strain trapezoids.

B. Characterizing Sensor Geometries

For the purposes of comparison, geometric tests of different $w \times t$ values are performed using lower strain trapezoids of 30%, over which range the responses are approximately linear: Fig. 3a. All of the samples are also found to give repeatable responses and be capable of withstanding strains of over 200% before delamination or fracture during tensile tests, and are thus all mechanically suitable for integration with the ring actuator. Therefore, selecting a particular geometry should depend on sensor response, durability, and convenience. In Fig. 3a, nine longitudinal geometries are tested: $w = 2, 4$, or 6 mm, and $t = 1, 2$, or 3 mm. The unstrained resistances behave as expected: local increases in w or t increase the sensory channel's cross-section and decrease the resistance. Only one exception exists ($t = 2$ mm, $w = 2 \rightarrow 4$ mm), which is assumed due to experimental deviations in the setup. Repeating these tests with more samples and averaging the results would be expected to eliminate this discrepancy. All nine sensors give clean and repeatable responses to the strain trapezoids, and Fig. 3b plots their sensitivities, calculated using the sensor's resistance values at 0% and 30% strain:

$$\frac{R_{30} - R_0}{R_0}. \quad (1)$$

Of the tested geometries, 4×3 mm gives the most significant sensitivity and is selected for subsequent tests. Though the trend of Fig. 3b suggests that greater t values would further increase the measured sensitivity, 3 mm is taken to be the maximum before the actuator's function is affected. Significant thicknesses should not be added to the surface of the actuator

since the channels might affect manipulation tasks or get caught more easily and initiate delamination. Similarly, wider channels would impact the composite sensor's ability to detect asymmetric deformations, which are explored in Section II-C.

C. Characterizing Asymmetric Deformations

The application of the composite sensors into the soft actuator (Section I) involves the detection of deformations perpendicular to the plane of the sensor, which we reproduce for characterization purposes using a representative probe fastened to a robotic arm (Fig. 4a). Since the out-of-plane deformations strain the material, we expect straightforward vertical deformations - positions A & B represent depressions of 10 & 15 mm, respectively - to be easily detectable. Indeed, the response of the straight longitudinal sensor in Fig. 4b demonstrates a marked difference in the measured resistances between positions O, A, & B, confirming the material's ability to detect these deformations.

However, this straight sensor morphology cannot discern the direction of asymmetric deformations (directions C & D in Fig. 4b, representative of the actuator's bifurcation directions), due to the symmetry of the sensorized strip; peaks C & D in the sensor's response are of very similar magnitude, despite representing displacements in opposite directions. To counter this and to add directionality information, asymmetries are introduced into the longitudinal sensor: Fig. 4 shows these new morphologies, referred to as square, circle, and triangle. Dimensions of each are given in Section IV. Fig. 4 plots their responses to identical deformations (with the synchronized square response also shown in the accompanying video).

In the responses of all three new morphologies, the difference between positions C & D is much clearer; the deformation in the direction of the additional material results in a significant resistance increase. The additional material means that purely vertical displacements produce a proportionally lesser response than the straight line, since the global strain increase is not as high. Still, deformations A & B produce clear responses in all tested samples. The square morphology is the only sample that decreases resistance after moving from A \rightarrow C; for the triangle, a slight increase occurs, whilst the stabilized values at A & C are very similar for the circle. Therefore, the square is the best choice for distinguishing between the two directions: at these representative deformations, the two respond of opposite signs and significantly different magnitude. By altering the morphology of a single sensor, 3 DoFs are achieved (elongation and two bending directions). The exact 2D deformation (vertical + lateral) cannot be inferred from the 1D response, but coupling the response with additional knowledge - such as multiple sensors and the applied pressure - a picture of an obscured actuator's state can be built.

The square morphology is the best choice for integration into the actuator, provided that the 90° corners of the square do not provide locations for stress concentrations to affect the material. Fig. 4c shows the results of tensile tests to failure on each of the four introduced sensor morphologies, on samples cast both transversely and longitudinally. The sites of delamination initiation are indicated on all - this

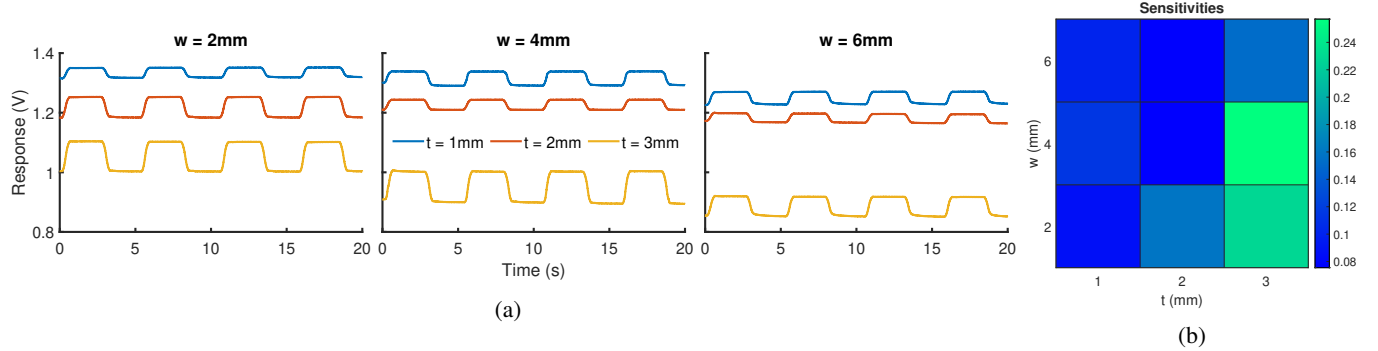


Fig. 3: a) Responses of the nine sensor geometries to a 30% applied trapezoidal strain. b) Sensitivities of the geometries during the trapezoidal tests: 4×3 mm & 2×3 mm demonstrate the highest values.

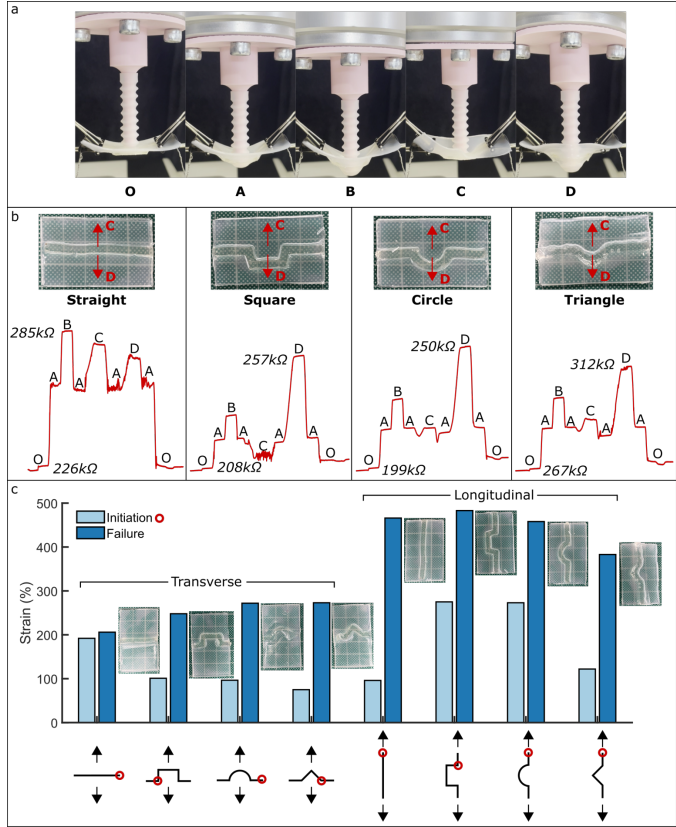


Fig. 4: Validation of the four sensor morphologies: straight, square, circle, and triangle. a) Experimental testing of the longitudinal morphologies' responses. A probe is used to apply out of the plane and asymmetric deformations. b) The responses of the longitudinal morphologies, with the asymmetric directions indicated; in all cases, 'D' is the deformation towards the side with additional material. c) Strain values at which the longitudinal and transverse sensors begin delamination and undergo complete failure. Red circles are used to indicate the initiation sites, which always occur at the clamped edge or a sharp corner.

always occurs either at the clamped edge, or at a cast corner, where the greatest stress concentrations. However, the square morphology does not cause any earlier failure than the other morphologies. Its additional material causes it to outlast the straight morphology to final failure, and it is selected for further tests. The square, circle, and triangle longitudinal morphologies do not stop functioning as sensors until $\geq 300\%$ strain.

D. Integration into Actuator

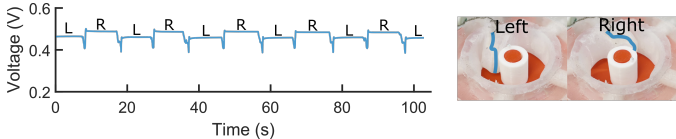
Based on the results of Section II-C, a hydrogel channel with the square morphology is embedded into the skin of the soft actuator (Fig. 5). For this preliminary demonstration of the composite sensor's capabilities, we detect the deformations of only one finger: in scaling the system, all five responses could be used alongside the applied pressure signals to define the actuator's state.

Fig. 5 validates the sensor's ability to detect the various deformations of a single finger. In 5a, the plot shows the capability of the single sensor morphology to detect asymmetries, as designed. The extended finger is manually oscillated between the left & right bistable states (with the position of the hydrogel channel overlaid in blue) when a cylinder of 17.5 mm diameter is centred in the actuator: the sensor can clearly distinguish between the two, and repeatably settles to raw voltages of 0.459 V & 0.487 V, respectively. Sharp decreases in resistance characterize the transition between the states, as the finger is forced backwards and the skin's strain is reduced.

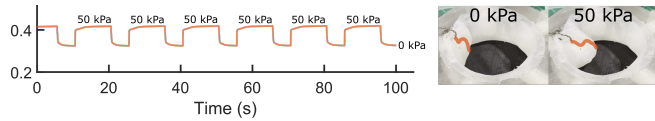
In Figs. 5b & 5c, the cylinder is removed and the finger is actuated via different pressure values between 10 kPa & 100 kPa. In the absence of an obstacle, the finger displaces radially, as illustrated in 5b. In this plot, the pressure is switched between 0 kPa & 50 kPa. The response quickly stabilizes when the state is switched, with no overshoots and negligible drift during the measured period. As the hydrogel maintains environmental equilibrium over longer time periods, the baseline (0 kPa) resistance is expected to drift; however, the local repeatability demonstrated here means that a brief application of known pressure values should be sufficient to recalibrate the sensor. Similarly, in Fig. 5c, 10 kPa steps are applied, and the difference in response between each is clearly distinguishable. The corresponding radial displacements of the finger for each pressure, measured from the ring's edge,

TABLE I: Radial displacements of the finger in Figs. 5b, 5c, & 6 over the range of applied pressures.

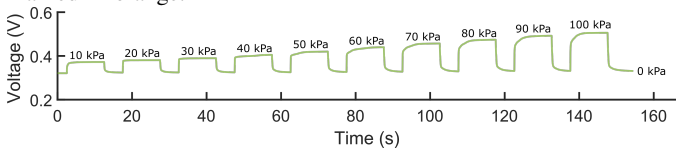
Pressure (kPa)	-80	-70	-60	-50	-40	-30	-20	-10	0	10	20	30	40	50	60	70	80	90	100
Displacement (mm)	8	9	9.5	9.5	9.5	10.5	12	13	13.5	14.5	16	17.5	18.5	19.5	20.5	21.5	22.5	23	23.5



(a) Asymmetric deformations. The position of the hydrogel channel is marked in blue.



(b) Repeated deformations. The position of the hydrogel channel is marked in orange.



(c) Applied pressures of increasing magnitude.

Fig. 5: Responses of a single sensorized finger integrated into the soft actuator. a) Bifurcations about a central cylinder. The finger is manually switched between the bistable states, which can be individually identified by the sensor. b) With no central cylinder, a pressure of 50 kPa is repeatedly applied to the finger. The response is highly repeatable, with no overshoot. c) With no central cylinder, pressures between 10 & 100 kPa are applied to the finger in 10 kPa increments. The embedded sensor identifies each value.

are presented in Table I. This table extends to include the application of 8 negative pressures, which draw the finger back into the body of the actuator. Fig. 6 uses this full range of available pressures during 10 triangular waves, mapping these to the resistive response of the finger. A kink in the response is seen during the transition from negative to positive applied pressure, where the hysteresis loops intersect, which is due to the skin's freedom of movement whilst no pressure is applied.

In Fig. 5, we see that a response of voltage 0.49 V could indicate both a rightwards bifurcation or a 90 kPa radial deformation. Given the single dimensionality of the sensor, it is not possible to distinguish between two such states from the stable value. However, information about the finger's path can be retrieved by analyzing the transient signals between 0 kPa and the deformed state. To illustrate this, Fig. 7 plots the response of the sensor in a series of 2 s cycles, where all 5 fingers are actuated to rotate the central cylinder about the vertical axis (see accompanying video). The sensor response is plotted (blue) in Fig. 7b, where the inwards travel of the finger (i.e. the ramps of increasing voltage) can be split into two approximately linear sections. The finger travels unobstructed radially before ~ 0.4 V and until the finger hits the cylinder. At this point, the finger bifurcates rightwards and continues

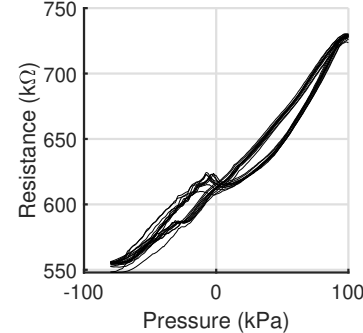


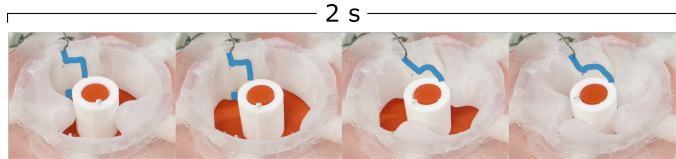
Fig. 6: The single finger's resistive response vs applied pressure, over 10 cycles of applied $-80 \rightarrow 100$ kPa triangular waves.

to extend, influencing the voltage to increase with a lesser gradient. When the cylinder is absent, and the same series of moves are performed (orange), no such shoulder occurs in the response, which smoothly levels out to the fully deformed value in a similar way to that seen in Figs. 5b & 5c. This means that two responses of otherwise identical magnitude can be separated between bifurcation and non-bifurcation cases by analyzing the transient instances. In the period between the two tests, the baseline resistance also shifts, highlighting the need for sensor calibration before proprioceptive sensing.

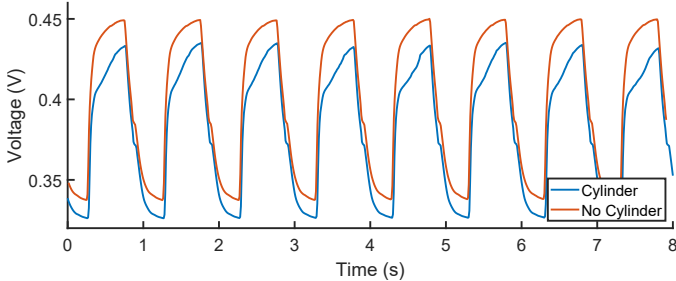
Fig 7c illustrates the loading phase of a ramp applied pressure to the soft finger and its interaction with three cylindrical objects of different diameters. The responses show where the interaction occurs, not to be confused with the kink in fig 6 as this happens under 0 kPa, while the hysteresis kink is shown when shifting between vacuum and applied pressure states. Although the raw sensor data is able to detect the interaction with objects, analysis of the transient and stable sensor responses can be performed by a neural network trained on a series of known deformations. The trained signals provide sufficient information for the finger's state - magnitude of deformation and whether/which direction bifurcation has occurred - can be extracted from the one-dimensional sensor response.

III. CONCLUSIONS

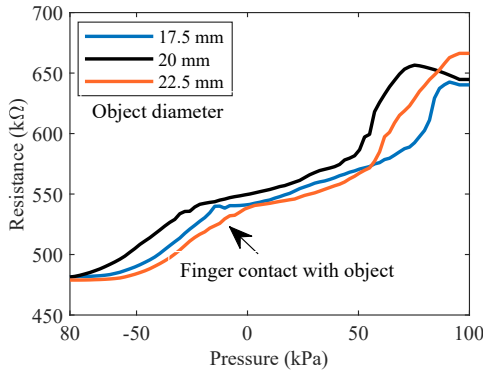
This work introduces a composite sensor consisting of a sensorized hydrogel channel encased in a silicone skin. It can repeatably and reliably respond to strain whilst remaining soft, stretchable, and flexible. The ability to cast or extrude both components introduces a significant level of customizability, enabling a range of sensor geometries and morphologies to be fabricated and tested straightforwardly. The total encasing of the hydrogel channel prevents delamination under repeated strain cycles, protects the hydrogel from fluctuations in environmental conditions, and maintains any implemented sensor morphologies during healing; therefore, excellent coupling properties. The composite sensors under characterization



(a) The 2 s periodic rotation cycle. The position of the hydrogel channel is marked in blue.



(b) The sensors's response to 8 complete periods of the cycle.



(c) The interaction of soft fingers with the cylindrical object of 3 different diameters.

Fig. 7: Coupled sensing of deformation and bifurcation direction. a) A periodic 2 s cycle during which the inner cylinder is rotated. b) 8 complete cycles, with (blue) and without (orange) the inner cylinder. A noticeable kink is visible when the cylinder is hit, and the finger is forced to change direction; as seen in Fig. 5a, the magnitude of this response can be used to deduce the bifurcation's presence & direction. c) The interaction between the finger and the object can be detected when the finger hits the object then start bending. The resistance of the three objects is varied related to their diameter, and the largest diameter forced the finger to bend earlier than the other two.

frequently undergo strains of over 200% before the onset of delamination; we also show how changes in the sensor morphology, such as the introduction of additional material to the longitudinal sensors, enables the sensor to continue partially functioning after delamination, avoiding complete failure until $\geq 386\%$ strain.

To illustrate the benefits provided by our composite sensors and the customizability which they provide, we present an exemplary process of soft morphology optimization for proprioceptive sensing in a soft actuator. Using characterization samples of appropriate dimensions, we select sensorized channels of 4×3 mm cross-sections, using this geometry

to fabricate and compare four asymmetric morphologies. Of these, the ‘square’ morphology best captures the asymmetric deformations C & D, whilst also remaining sensitive to purely perpendicular deformations. In the longitudinal configuration, this morphology is shown to undergo 275% applied strain before the initiation of delamination, demonstrating its potential to be incorporated as a sensing approach into a large range of soft robotic actuators without risk of delamination. The chosen geometry and morphology excellently perform when incorporated into the soft actuator, clearly showing distinctions between the bifurcation states and 11 different pressure values during radial deformation. Notably, we present our preliminary findings of the use of transient analysis to extract the state of the underactuated manipulator, demonstrating a clear difference in signal when a 17.5 mm cylinder is present during periodically applied pressures. Further work will seek to extract these transient effects by training a neural network to recognize the different transient states and constant values, aiming to identify the shapes and sizes of different objects in the manipulator by combining the information from multiple sensors, coupling machine learning techniques with morphology-level optimization in order to extract significant levels of proprioceptive data from simple sensor implementations.

IV. MATERIALS AND METHODS

All characterization samples are fabricated from a combination of platinum-catalyzed silicone (Ecoflex 0030 and Slacker with a mix ratio of 1:0.5, Smooth-On) and a sensorized gelatin/glycerol hydrogel. The composition of the ionically sensorized gelatin/glycerol hydrogel is taken from the authors’ previous work [22], and is mixed in the mass ratio 1:1.5:2.5:0.2:0.1 Ge:Gl:H₂O:CA:NaCl, where Ge → 240/260 pork gelatin powder (*Cake SOS*), Gl → glycerol (*Fisher Scientific*), CA → citric acid monohydrate (*Fisher Scientific*), and NaCl → sodium chloride-based table salt (*Sainsbury’s*). Coldwater is first poured onto the gelatin powder in a glass beaker and left to bloom for 10 minutes before Gl, CA, & NaCl are added. The beaker is covered with parafilm to minimize evaporation, and transferred to a 50°C water bath. Once the mixture homogenizes, the bath is used to maintain the sol state for casting: the sol-gel transition occurs at ~45°C. After casting, the hydrogel loses water to reach an environmental equilibrium, where it remains flexible and stretchable: all cast samples are left for at least 24 hours before encasing/testing in order to facilitate this. Once cured, the hydrogel behaves as a strain sensor, linearly increasing its resistance as a unidirectional strain is applied.

To fabricate each sample, soft skin is first cast into a 50×30×1 mm mould, which is 3D printed from polylactic acid (PLA). This is left to cure overnight before a hydrogel strip of the desired shape/dimension is cast onto its free surface at 50°C, using an additional PLA template (t mm thickness) to mask the areas which should not be sensorized. This mask is either longitudinal (the sensorized strip covers the entire 50 mm length) or transverse (the 30 mm length, matching the width of the soft actuator’s skin). The excess mixture is scraped from the mask using a razor blade, and the sample

is left for 24 hours at room temperature before the mask is removed, and a thin layer of silicone (same mix as soft skin) is cast to encase the hydrogel strip (Fig. 2a). Simply, the mixture pours over the sensor to provide a thin film, while the excessive mixture is removed by a razor blade. When measuring the resistance of a sample, silver conductive yarn is sewed through the sensorized channel 5 mm from its edges, which is connected to the measurement circuit. During the geometry characterizations of Fig. 3, the conductive yarn is replaced with solid core wire, stripped at both ends.

The alternating current (AC) impedance of all tests is measured with a 100 kHz sampling rate, using a *National Instruments* USB-6212 multifunction I/O device. A 10 kHz sine wave between ± 2 V is applied across a potential divider, with one side of the sensor connected to the ground and a matched resistor joining this to the USB-6212's output, such that an increase in the sensor's resistance results in an increased peak-to-peak measurement at the measured node. During the geometry tests (Fig. 3), the upper resistor is 220 k Ω ; in Fig. 4's morphology tests, 680 k Ω is used; and during the actuator's characterization (Figs. 5 & 7), this is 160 k Ω . All plotted responses are the upper envelope of the measured response, smoothed using a 1000-sample rolling window. Small phase shifts between input and output are ignored; we do not explicitly consider any high-frequency capacitive effects. Before measurements are taken, a shorted circuit is analyzed to approximate a 272 Ω background resistance in the setup. Since this is negligible compared to the $\sim 10^5$ Ω measured responses, this is not considered further.

Tensile tests are performed by first clamping 10 mm of each sample's ends (Fig. 2a's shaded region). One clamp is secured to the table, whilst the other is attached to a *Universal Robots* UR5 robot arm, programmed to move only in the vertical axis. Strain values are calculated from the 30 mm unstressed length. All trapezoids are applied at 30 mms $^{-1}$, whilst uniaxial failure tests use a more quasistatic 5mms $^{-1}$ rate. The strains in Fig. 4c are calculated from video footage of the tensile tests, using the UR5's known constant speed. Initiation is taken to occur at the first visible evidence of fracture or delamination, whilst failure is defined as the point at which the sample no longer functions as a strain sensor, whether due to delamination of the soft skin/hydrogel bond or total fracture of the specimen.

Out-of-plane deformation tests of the longitudinal sensors (Fig. 4a & b) are also performed using a UR5 arm, equipped with a 3D printed PLA end effector (Fig. 4). The 6 mm diameter probe is covered with one of the ring actuator's bellows in order to best replicate the deformations expected during integration with the actuator. Positions A & B represent vertical deformations of 10 & 15 mm, respectively, whilst positions C & start at position A before rotating 0.1 radians about an axis 167.5 mm above the longitudinal sensor (i.e. parallel to the plane of Fig. 4a's photos), which drags the centre transversely along a 17.65 mm arc length. Fig. 4b illustrates the directions of these deformations relative to the longitudinal morphologies under consideration, as well as the order in which the positions are visited during characterization. 2 s pauses are implemented between each move, with maximum velocities and accelerations limited to 50mms $^{-1}$ and

100mms $^{-2}$, respectively. All of the asymmetric morphologies are cast with a 4 \times 3 mm channel, with the channels passing through a point transversely offset by 7.5 mm from the centre of the 50 mm length. All are straight for the first 17.5 mm from either end, necessitating a semicircle of radius 7.5 mm, a 'triangle' of side length 10.6 mm, and a rectangle with side lengths 15 mm and 7.5 mm.

To implement the sensor in the soft skin of the ring actuator, a similar method of casting the soft skin, sensor, and then the thin film is accomplished. Soft skin with embedded hydrogel sensor is shown in fig 1. The sensor is centred and placed in front of a soft finger. The fabrication procedure of the ring actuator is followed similar to [1]. Briefly, each cap of the soft fingers is glued with the soft skin with silicone glue (sil-poxy, Smooth-On). To control the soft fingers, we used the same setup provided in [1], [36].

ACKNOWLEDGEMENTS

This work was supported by the SHERO project, a Future and Emerging Technologies (FET) programme of the European Commission (grant agreement ID 828818), and by EPSRC's RoboPatient EP/T00519X/1 and EP/R513180/1 DTP.

AUTHOR DISCLOSURE STATEMENT

The authors declare no competing interests.

REFERENCES

- [1] R. Hashem, S. Kazemi, M. Stommel, L. K. Cheng, and W. Xu, "A biologically inspired ring-shaped soft pneumatic actuator for large deformations," *Soft Robotics*, 2021.
- [2] D. Rus and M. T. Tolley, "Design, fabrication and control of soft robots," *Nature*, vol. 521, no. 7553, pp. 467–475, 2015.
- [3] M. Amjadi, K.-U. Kyung, I. Park, and M. Sitti, "Stretchable, skin-mountable, and wearable strain sensors and their potential applications: a review," *Advanced Functional Materials*, vol. 26, no. 11, pp. 1678–1698, 2016.
- [4] C. Mattmann, F. Clemens, and G. Tröster, "Sensor for measuring strain in textile," *Sensors*, vol. 8, no. 6, pp. 3719–3732, 2008.
- [5] A. Georgopoulou and F. Clemens, "Piezoresistive Elastomer-Based Composite Strain Sensors and Their Applications," *ACS Applied Electronic Materials*, vol. 2, no. 7, pp. 1826–1842, 2020.
- [6] S. Sareh, A. Jiang, A. Faragasso, Y. Noh, T. Nanayakkara, P. Dasgupta, L. D. Seneviratne, H. A. Wurdemann, and K. Althoefer, "Bio-inspired tactile sensor sleeve for surgical soft manipulators," in *2014 IEEE International Conference on Robotics and Automation (ICRA)*, pp. 1454–1459, IEEE, 2014.
- [7] Y.-L. Park, B.-R. Chen, and R. J. Wood, "Design and fabrication of soft artificial skin using embedded microchannels and liquid conductors," *IEEE Sensors Journal*, vol. 12, no. 8, pp. 2711–2718, 2012.
- [8] R. K. Kramer, C. Majidi, R. Sahai, and R. J. Wood, "Soft curvature sensors for joint angle proprioception," in *2011 IEEE/RSJ International Conference on Intelligent Robots and Systems*, pp. 1919–1926, IEEE, 2011.
- [9] H. Zhao, J. Jalving, R. Huang, R. Knepper, A. Ruina, and R. Shepherd, "A helping hand: Soft orthosis with integrated optical strain sensors and eng control," *IEEE Robotics & Automation Magazine*, vol. 23, no. 3, pp. 55–64, 2016.
- [10] A. Georgopoulou, S. Michel, and F. Clemens, "Sensorized robotic skin based on piezoresistive sensor fiber composites produced with injection molding of liquid silicone," *Polymers*, vol. 13, no. 8, 2021.
- [11] T. Hainsworth, L. Smith, S. Alexander, and R. MacCurdy, "A Fabrication Free, 3D Printed, Multi-Material, Self-Sensing Soft Actuator," *IEEE Robotics and Automation Letters*, vol. 5, no. 3, pp. 4118–4125, 2020.
- [12] H. Banerjee, M. Suhail, and H. Ren, "Hydrogel actuators and sensors for biomedical soft robots: brief overview with impending challenges," *Biomimetics*, vol. 3, no. 3, p. 15, 2018.

- [13] Y. Lee, W. Song, and J.-Y. Sun, "Hydrogel soft robotics," *Materials Today Physics*, vol. 15, p. 100258, 2020.
- [14] P. He, J. Wu, X. Pan, L. Chen, K. Liu, H. Gao, H. Wu, S. Cao, L. Huang, and Y. Ni, "Anti-freezing and moisturizing conductive hydrogels for strain sensing and moist-electric generation applications," *Journal of Materials Chemistry A*, vol. 8, no. 6, pp. 3109–3118, 2020.
- [15] G. Cai, J. Wang, K. Qian, J. Chen, S. Li, and P. S. Lee, "Extremely stretchable strain sensors based on conductive self-healing dynamic cross-links hydrogels for human-motion detection," *Advanced Science*, vol. 4, no. 2, p. 1600190, 2017.
- [16] Y.-J. Liu, W.-T. Cao, M.-G. Ma, and P. Wan, "Ultrasensitive wearable soft strain sensors of conductive, self-healing, and elastic hydrogels with synergistic "soft and hard" hybrid networks," *ACS applied materials & interfaces*, vol. 9, no. 30, pp. 25559–25570, 2017.
- [17] Z. Shao, X. Hu, W. Cheng, Y. Zhao, J. Hou, M. Wu, D. Xue, and Y. Wang, "Degradable self-adhesive epidermal sensors prepared from conductive nanocomposite hydrogel," *Nanoscale*, 2020.
- [18] J. Shintake, H. Sonar, E. Piskarev, J. Paik, and D. Floreano, "Soft pneumatic gelatin actuator for edible robotics," in *2017 IEEE/RSJ International Conference on Intelligent Robots and Systems (IROS)*, pp. 6221–6226, IEEE, 2017.
- [19] A. N. Sardesai, X. M. Segel, M. N. Baumholtz, Y. Chen, R. Sun, B. W. Schork, R. Buonocore, K. O. Wagner, and H. M. Golecki, "Design and Characterization of Edible Soft Robotic Candy Actuators," *MRS Advances*, vol. 3, no. 50, pp. 3003–3009, 2018.
- [20] M. Baumgartner, F. Hartmann, M. Drack, D. Preninger, D. Wirthl, R. Gerstmayr, L. Lehner, G. Mao, R. Pruckner, S. Demchyshyn, L. Reiter, M. Strobel, T. Stockinger, D. Schiller, S. Kimeswenger, F. Greibich, G. Buchberger, E. Bradt, S. Hild, S. Bauer, and M. Kaltenbrunner, "Resilient yet entirely degradable gelatin-based biogels for soft robots and electronics," *Nature Materials*, vol. 19, no. 10, pp. 1102–1109, 2020.
- [21] M. K. A. Heiden, D. Preninger, L. Lehner, M. Baumgartner, M. Drack, E. Woritzka, D. Schiller, R. Gerstmayr, F. Hartmann, "3D-printing of resilient biogels for omnidirectional and exteroceptive soft actuators," *Science Robotics*, vol. 2119, no. February, pp. 1–11, 2022.
- [22] D. Hardman, T. George Thuruthel, and F. Iida, "Self-healing ionic gelatin/glycerol hydrogels for strain sensing applications," *NPG Asia Materials*, vol. 14, 2022.
- [23] J. Hughes and D. Rus, "Mechanically Programmable, Degradable Ingestible Soft Actuators," *2020 3rd IEEE International Conference on Soft Robotics, RoboSoft 2020*, pp. 836–843, 2020.
- [24] T. Nagai, A. Kurita, and J. Shintake, "Characterization of sustainable robotic materials and finite element analysis of soft actuators under biodegradation," *Frontiers in Robotics and AI*, vol. 8, p. 383, 2021.
- [25] D. Hardman, J. Hughes, T. G. Thuruthel, K. Gilday, and F. Iida, "3d printable sensorized soft gelatin hydrogel for multi-material soft structures," *IEEE Robotics and Automation Letters*, 2021.
- [26] J. T. Muth, D. M. Vogt, R. L. Truby, Y. Mengüç, D. B. Kolesky, R. J. Wood, and J. A. Lewis, "Embedded 3d printing of strain sensors within highly stretchable elastomers," *Advanced materials*, vol. 26, no. 36, pp. 6307–6312, 2014.
- [27] R. L. Truby and J. A. Lewis, "Printing soft matter in three dimensions," *Nature*, vol. 540, no. 7633, pp. 371–378, 2016.
- [28] S. Liu and L. Li, "Ultrastretchable and self-healing double-network hydrogel for 3D printing and strain sensor," *ACS Applied Materials & Interfaces*, vol. 9, no. 31, pp. 26429–26437, 2017.
- [29] Z. Lei, Q. Wang, and P. Wu, "A multifunctional skin-like sensor based on a 3d printed thermo-responsive hydrogel," *Materials Horizons*, vol. 4, no. 4, pp. 694–700, 2017.
- [30] K. Tian, J. Bae, S. E. Bakarich, C. Yang, R. D. Gately, G. M. Spinks, M. In Het Panhuis, Z. Suo, and J. J. Vlassak, "3d printing of transparent and conductive heterogeneous hydrogel–elastomer systems," *Advanced Materials*, vol. 29, no. 10, p. 1604827, 2017.
- [31] W. Sun, S. Schaffer, K. Dai, L. Yao, and A. Feinberg, "3D Printing Hydrogel-Based Soft and Biohybrid Actuators : A Mini-Review on Fabrication Techniques , Applications , and Challenges," *Frontiers in Robotics and AI*, vol. 8, no. April, pp. 1–10, 2021.
- [32] S. Terryn, J. Langenbach, E. Roels, J. Brancart, C. Bakkali-Hassani, Q.-A. Poutrel, A. Georgopoulou, T. G. Thuruthel, A. Safaei, P. Ferrentino, et al., "A review on self-healing polymers for soft robotics," *Materials Today*, 2021.
- [33] E. Roels, S. Terryn, J. Brancart, R. Verhelle, G. V. Assche, and B. Vanderborght, "Additive Manufacturing for Self-Healing Soft Robots," vol. 00, no. 00, pp. 1–13, 2020.
- [34] M. Khatib, O. Zohar, and H. Haick, "Self-healing soft sensors: from material design to implementation," *Advanced Materials*, vol. 33, no. 11, p. 2004190, 2021.
- [35] J. Kang, J. B.-H. Tok, and Z. Bao, "Self-healing soft electronics," *Nature Electronics*, vol. 2, no. 4, pp. 144–150, 2019.
- [36] R. Hashem and F. Iida, "Embedded soft sensing in soft ring actuator for aiding with the self-organisation of the in-hand rotational manipulation," *IEEE International Conference on Soft Robotics 2022 (RoboSoft'22)*, Accepted, 2022.